

CNN-based InSAR Coherence Classification

Subhayan Mukherjee¹, Aaron Zimmer², Xinyao Sun¹, Parwant Ghuman², Irene Cheng¹

¹Department of Computing Science, University of Alberta, Edmonton, Canada

²3v Geomatics, Vancouver, Canada

{mukherje, xinyao1, locheng}@ualberta.ca

{azimmer, pghuman}@3vgeomatics.com

Abstract—Interferometric Synthetic Aperture Radar (InSAR) imagery based on microwaves reflected off ground targets is becoming increasingly important in remote sensing for ground movement estimation. However, the reflections are contaminated by noise, which distorts the signal’s wrapped phase. Demarcation of image regions based on degree of contamination (“coherence”) is an important component of the InSAR processing pipeline. We introduce Convolutional Neural Networks (CNNs) to this problem domain and show their effectiveness in improving coherence-based demarcation and reducing misclassifications in completely incoherent regions through intelligent preprocessing of training data. Quantitative and qualitative comparisons prove superiority of proposed method over three established methods.

Keywords—InSAR; Markov Random Field; coherence; classification; Convolutional Neural Networks

I. INTRODUCTION

In the past few decades, there has been an increasing use of remote sensing using activate microwave in general, and Synthetic Aperture Radar Interferometry (InSAR) in particular. The phase component of InSAR signal encodes the distance between satellite and ground target, and phase unwrapping can help create highly accurate Digital Elevation Maps (DEMs). Unfortunately, the phase data often suffers contamination due to noise arising from numerous sources, e.g. atmospheric factors. Hence, denoising of the phase prior to unwrapping is essential to optimize the InSAR processing pipeline as a whole.

Ground images acquired using InSAR are “non-stationary” due to changes in topography and displacement of ground along the satellite’s line of sight. The boxcar filtering approach, which is still widely used today, involves computing moving average using a rectangular window. But the non-stationary nature of InSAR signal adversely affects the performance of sample average methods like boxcar [1]. Also, the strong smoothing effect of boxcar filtering renders spatial resolution loss, in addition to noticeable phase and coherence estimation errors near signal discontinuities. Consequently, various filtering methods have tried to address this problem of estimating non-stationary InSAR phase. These methods are broadly classified as spatial methods, e.g., Lee [2], and frequency-based methods, e.g., Goldstein [3]. Both of these filters, as well as [4] are adaptive to local fringe direction. The original and modified Goldstein filter of Baran et al. [5] preserves the signal in high coherence (low noise) areas, which makes them locally noise-adaptive as well. This emphasizes the importance of accurate classification of image regions based on coherence. Lee filter’s enhancements [6-9] improve

adaptation to the fringe structure in the local signal neighborhood, whereas modifications to the Goldstein and Baran filters avoid under-filtering the incoherent regions via improved coherence estimation [10, 11]. Other approaches include wavelet domain methods [12] including un-decimated wavelet transform [13] and wavelet packets [14], local modeling based on polynomial approximation [15], sparse coding [16], Markov Random Field (MRF) based methods [17, 18] (though prior distribution modeling required in MRF is difficult) and non-local filtering methods [19-21].

While Neural Network based SAR images despeckling [22-25] and improvement of geo-localization accuracy for optical satellite images [26] have been explored, Convolutional Neural Network (CNN) based learning approaches to InSAR images’ coherence classification have not been investigated. This paper proposes coherence classification using a CNN. We show how intelligent MRF-based preprocessing of raw coherence can train the coherence classifier CNN to improve demarcation of coherent and incoherent regions in the input noisy interferogram, and also reduce misclassifications in completely incoherent regions, which is ubiquitous in methods like boxcar.

Our work is distinct from [17, 18] in that we use MRF for thresholding the raw coherence while preparing training labels. In contrast, the authors in [17, 18] use MRF for denoising. Our work is also different from [27-32], as the type of data we use is InSAR, not (Pol)SAR, and our objective is not classifying ground targets, but separating coherent and incoherent regions.

II. PROPOSED METHOD

Fig. 1 shows our coherence classification CNN. We do not need to constrain the network’s training image size or that for running inference using the network after training. We can use patches or whole image as input. The CNN has two input channels, representing real and imaginary components of the complex interferogram image. Thus, information from both channels is used simultaneously. First, they are considered separately to saturate outlier amplitudes (some input interferogram pixels might have extremely high amplitudes, which can degrade the training / inference). Let interferogram pixels be $Z = [z_1, z_2, \dots, z_N]$ having amplitudes $A = [a_1, a_2, \dots, a_N]$. Amplitude of each pixel can be thresholded as $A' = \text{saturate}(A, M)$, where M is the mask representing outlier amplitudes. The outliers are computed following the method [33]. We saturate and normalize real and imaginary channel values to lie between -1 and +1. We then add 1 to each channel in order to use the Rectified Linear Unit (ReLU) activation for introducing nonlinearity in the CNN to learn complex features.

In Fig.1, each box represents a CNN layer. The integer at the top (1, 16) represents the number of output feature maps, whereas filter dimension is mentioned at the bottom (3×3). Each 2D convolutional layer learns a number of filters. We use separable convolutions to reduce the number of weights to be trained for faster convergence. The output of the last convolutional layer is a single channel, as we need to classify each pixel based on only its coherence's amplitude. The activation for final convolution layer is sigmoid instead of ReLU because, pixel coherence is a value between 0 and 1 (sigmoid output). Binary Cross-entropy between the output channel and the training target is reduced using the popular Adam optimizer to train the network, by updating its filter weights and biases, using gradient backpropagation. The Xavier method [34] is used to initialize the weights of the CNN before training starts. We similarly build another CNN to filter the noisy interferograms. It has an autoencoder structure of 3×3 filters [16-8-Maxpool-8-Upsample-16-2] with ReLU activation even on the last layer. Maxpooling layers subsample their input feature maps by a factor of 3; Upsampling layers bring them back to their original size. The last convolutional layer has two output feature maps (real and imaginary channels of output). This filtering/denoising CNN is trained to reduce mean squared error between output and input channels via Adam optimizer.

We extract corresponding 64×64 patches from each real-world noisy training image and its thresholded coherence to train the coherence classification CNN. The method used to threshold the raw coherence is described in detail next.

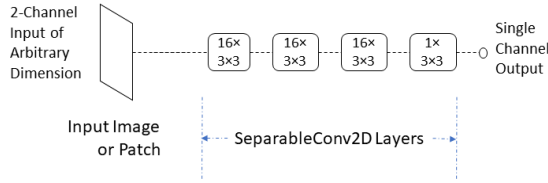


Fig. 1: Proposed CNN for InSAR coherence classification.

To train the CNN in Fig. 1, we first extract 7×7 patches and compute the raw coherence between the training noisy images and their filtered version output by the fully trained filtering network described earlier. Raw coherence is defined in Eq. 1:

$$\hat{\gamma} = \frac{\sum_{n,m} u_1(n,m) \cdot u_2^*(n,m) \cdot e^{-j\phi(n,m)}}{\sqrt{\sum_{n,m} |u_1(n,m)|^2 \sum_{n,m} |u_2(n,m)|^2}} \quad (1)$$

where pixel n of interferogram u_1 and pixel m of interferogram u_2 have the angle of separation Φ , and the asterisk on top of u_2 denotes complex conjugate. A relatively large patch size (7×7) is used to reduce bias in raw coherence computation.

Next, for thresholding the raw coherence, we employ a Markov Random Field (MRF) based approach. Advantages of choosing MRF over simple histogram-based thresholding are: (a) spatial context is taken into consideration, and (b) smoothness of the thresholded regions (coherent and incoherent) can be adjusted by tuning a single parameter, as shown later. First, we initialize the pixel-wise estimates for the MRF using a fixed threshold. It was observed by running Otsu's global thresholding [35] on several raw coherence images that the average threshold is 0.6. Thus, we used 0.6 as the fixed threshold, such that pixel values above it are considered coherent (set to 1) and below it as

incoherent (set to 0). Given these initial estimates $\{P_{ij} : 0 \text{ or } 1\}$, we try to find a solution $\{S_{ij} : 0 \text{ or } 1\}$ that minimizes Eq. 2

$$\sum_{ij} |P_{ij} - S_{ij}| + \sum_{ij} \sum_{kl} (\alpha * |S_{ij} - S_{(i+k)(j+l)}|) \quad (2)$$

where α is the smoothness parameter that needs to be manually tuned based on the results, and $||$ is the L_1 norm. Also, k and l represent indices of pixel neighborhood. Since this is a binary classification (false:0 / true:1), exact solution for the expression in Eq. 2 was found via graph-cut optimization [36]. In Fig. 2, we show result of thresholding raw coherence by MRF for a sample training image. Black and white pixels represent 0 (low coherence) and 1 (high coherence) respectively. The value of $\alpha = 2.5$ was experimentally found to produce this best result.

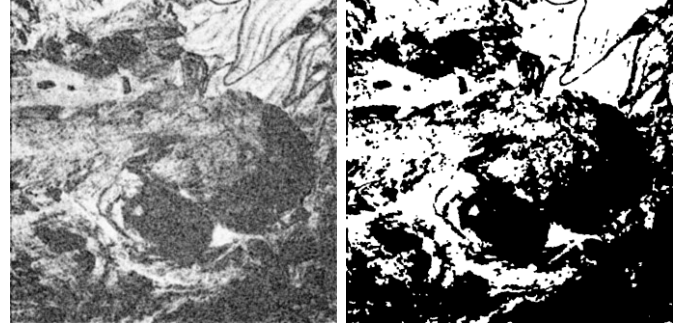
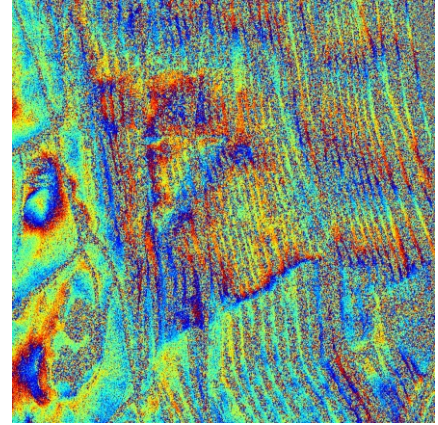


Fig. 2: Threshold raw 7×7 coherence via MRF and graph-cut.



(a) Input Interferogram (Phase); Blue: $-\pi$; Red: $+\pi$



(b) Boxcar Coherence Output (Run time: 1.32 sec)



(c) NLIInSAR Coherence Output [37] (Run time: 20.44 sec)



(d) NLSAR Coherence Output [38] (Run time: 11.49 sec)



(e) Proposed Method Coherence Output (Run time: 0.67 sec)

Fig. 3: Coherence classification of proposed vs. established methods: -ve (black: incoherent) and +ve (white: coherent).

III. RESULTS AND DISCUSSION

We implemented both networks (described earlier) using Keras with Tensorflow back-end. We trained the filtering CNN and coherence classifier CNN by extracting 500 60×60 sized and 64×64 sized patches respectively from each of 135 1000×1000 training interferograms. We used a large batch size of 100 to prevent overfitting. We started the training with learning rate 10^{-3} and halved it every 10 epochs for fast convergence. The

CNNs converged after 50 and 100 epochs respectively. The trained CNNs were tested on 1000×1000 interferograms from a different geographic location, but using the interferogram itself as input, instead of just patches. Fig. 3 compares our method's coherence and run time performance with 3 existing methods.

Comparing outputs of all four methods against the input noisy interferogram in Fig 3a, we see that our method creates better, more accurate demarcation between coherent and incoherent regions, and lesser coherence misclassifications in completely incoherent areas than both Boxcar and NLSAR [37]. Our method does not have image border artefacts or false positives along borders of incoherent regions like NLIInSAR [38]. A key advantage of our approach is: we can tune a single smoothness parameter as per the application requirements, while preparing training data to control the degree of smoothness of coherence classifications. Fig. 2 indicates that our method can be improved further by lowering bias in raw coherence. We multiply the input interferogram with its filtered version's complex conjugate to prevent the signals from biasing down coherence estimates, but we also found that wherever filtering fails to denoise properly, this process cancels out noise in noisy areas where some noise is still left in the filtered version. This drives up coherence. Thus, we can further reduce false positive classifications via better filtering. Also, the execution time of our classifier CNN is only 0.67 seconds, which is far less than other methods. All methods were implemented and executed in OpenCL 1.2 on a NVIDIA 1070 GPU with 8 GB GPU RAM.

To further validate our method, we simulated 100 clean ground truth interferograms with Gaussian bubbles, roads and buildings, added Gaussian noise, and input noisy versions to each method mentioned in Fig. 3, including ours. Performance score of each method's coherence classification with respect to ground truth classification for threshold = 0.6 are presented in Table I. Similarly, preprocessing accuracy, precision and recall were evaluated to be about 82, 80 and 95 percent respectively, and these confirmed the classifier CNN's training convergence.

TABLE I. AVERAGED SCORES ON 100 SIMULATED INTERFEROGRAMS

Metric	<i>Boxcar</i>	<i>NLIInSAR</i>	<i>NLSAR</i>	<i>Proposed</i>
accuracy	0.8008	0.8273	0.4951	0.8425
precision	0.8248	0.8126	0.7389	0.8399
recall	0.8522	0.9265	0.2983	0.9107

Table I shows how our method outperforms others; NLIInSAR recall is slightly higher, but we deduced from its output images that this is an anomaly, because it just overestimates coherence. Still, bias reduction in raw coherence computation and fine-tuning MRF thresholding to reduce resolution loss can generate even better results in our method, which is over 30 times faster than its closest rival, NLIInSAR as per real and simulated data.

IV. CONCLUSION

We propose a CNN-based coherence classifier for InSAR images. It creates far less misclassifications in incoherent areas than existing methods, and outperforms its closest competitor, NLIInSAR by 30 times in run time. These show the capability of CNN-based learning for InSAR coherence classification.

REFERENCES

- [1] M. S. Seymour and I. G. Cumming, "Maximum likelihood estimation for SAR interferometry," in *Proc. IEEE Int. Geosci. Remote Sens. Symp.*, Aug. 1994, pp. 2272–2275.
- [2] J.-S. Lee, K. P. Papathanassiou, T. L. Ainsworth, M. R. Grunes, and A. Reigber, "A new technique for noise filtering of SAR interferometric phase images," *IEEE Trans. Geosci. Remote Sens.*, vol. 36, no. 5, pp. 1456–1465, Sep. 1998.
- [3] R. M. Goldstein and C. L. Werner, "Radar interferogram filtering for geophysical applications," *Geophys. Res. Lett.*, vol. 25, no. 21, pp. 4035–4038, Nov. 1998.
- [4] E. Trouvé, J.-M. Nicolas, and H. Maître, "Improving phase unwrapping techniques by the use of local frequency estimates," *IEEE Trans. Geosci. Remote Sens.*, vol. 36, no. 6, pp. 1963–1972, Nov. 1998.
- [5] I. Baran, M. P. Stewart, B. M. Kampes, Z. Perski, and P. Lilly, "A modification to the Goldstein radar interferogram filter," *IEEE Trans. Geosci. Remote Sens.*, vol. 41, no. 9, pp. 2114–2118, Sep. 2003.
- [6] N. Wu, D.-Z. Feng, and J. Li, "A locally adaptive filter of interferometric phase images," *IEEE Geosci. Remote Sens. Lett.*, vol. 3, no. 1, pp. 73–77, Jan. 2006.
- [7] S. Fu, X. Long, X. Yang, and Q. Yu, "Directionally adaptive filter for synthetic aperture radar interferometric phase images," *IEEE Trans. Geosci. Remote Sens.*, vol. 51, no. 1, pp. 552–559, Jan. 2013.
- [8] C.-F. Chao, K.-S. Chen, and J.-S. Lee, "Refined filtering of interferometric phase from InSAR data," *IEEE Trans. Geosci. Remote Sens.*, vol. 51, no. 12, pp. 5315–5323, Dec. 2013.
- [9] G. Vasile, E. Trouvé, J.-S. Lee, and V. Buzuloiu, "Intensity-driven adaptive-neighborhood technique for polarimetric and interferometric SAR parameters estimation," *IEEE Trans. Geosci. Remote Sens.*, vol. 44, no. 6, pp. 1609–1621, Jun. 2006.
- [10] R. Song, H. Guo, G. Liu, Z. Perski, and J. Fan, "Improved Goldstein SAR interferogram filter based on empirical mode decomposition," *IEEE Geosci. Remote Sens. Lett.*, vol. 11, no. 2, pp. 399–403, Feb. 2014.
- [11] M. Jiang *et al.*, "The improvement for Baran phase filter derived from unbiased InSAR coherence," *IEEE J. Sel. Topics Appl. Earth Observ. Remote Sens.*, vol. 7, no. 7, pp. 3002–3010, Jul. 2014.
- [12] C. Lopez-Martinez and X. Fabregas, "Modeling and reduction of SAR interferometric phase noise in the wavelet domain," *IEEE Trans. Geosci. Remote Sens.*, vol. 40, no. 12, pp. 2553–2566, Dec. 2002.
- [13] Y. Bian and B. Mercer, "Interferometric SAR phase filtering in the wavelet domain using simultaneous detection and estimation," *IEEE Trans. Geosci. Remote Sens.*, vol. 49, no. 4, pp. 1396–1416, Apr. 2011.
- [14] X. Zha, R. Fu, Z. Dai, and B. Liu, "Noise reduction in interferograms using the wavelet packet transform and Wiener filtering," *IEEE Geosci. Remote Sens. Lett.*, vol. 5, no. 3, pp. 404–408, Jul. 2008.
- [15] J. Bioucas-Dias, V. Katkovnik, J. Astola, and K. Egiazarian, "Absolute phase estimation: Adaptive local denoising and global unwrapping," *Appl. Opt.*, vol. 47, no. 29, pp. 5358–5369, 2008.
- [16] H. Hongxing, J. M. Bioucas-Dias, and V. Katkovnik, "Interferometric phase image estimation via sparse coding in the complex domain," *IEEE Trans. Geosci. Remote Sens.*, vol. 53, no. 5, pp. 2587–2602, May 2015.
- [17] G. Ferraiuolo and G. Poggi, "A Bayesian filtering technique for SAR interferometric phase fields," *IEEE Trans. Image Process.*, vol. 13, no. 10, pp. 1368–1378, Oct. 2004.
- [18] L. Denis, F. Tupin, J. Darbon, and M. Sigelle, "Joint regularization of phase and amplitude of InSAR data: Application to 3-D reconstruction," *IEEE Trans. Geosci. Remote Sens.*, vol. 47, no. 11, pp. 3774–3785, Nov. 2009.
- [19] A. Buades, B. Coll, and J.-M. Morel, "A review of image denoising algorithms, with a new one," *Multiscale Model. Simul.*, vol. 4, no. 2, pp. 490–530, 2005.
- [20] C.-A. Deledalle, L. Denis, G. Poggi, F. Tupin, and L. Verdoliva, "Exploiting patch similarity for SAR image processing: The nonlocal paradigm," *IEEE Signal Process. Mag.*, vol. 31, no. 4, pp. 69–78, Jul. 2014.
- [21] F. Sica, D. Cozzolino, X. X. Zhu, L. Verdoliva and G. Poggi, "InSAR-BM3D: A Nonlocal Filter for SAR Interferometric Phase Restoration," in *IEEE Transactions on Geoscience and Remote Sensing*, vol. 56, no. 6, pp. 3456–3467, June 2018.
- [22] P. Wang, H. Zhang and V. M. Patel, "Generative adversarial network-based restoration of speckled SAR images," *2017 IEEE 7th International Workshop on Computational Advances in Multi-Sensor Adaptive Processing (CAMSAP)*, Curacao, 2017, pp. 1–5.
- [23] X. Tang, L. Zhang, and X. Ding, "SAR image despeckling with a multilayer perceptron neural network," *International Journal of Digital Earth*, pp. 1–21, Aug. 2018.
- [24] P. Wang, H. Zhang, and V. M. Patel, "SAR Image Despeckling Using a Convolutional Neural Network," *IEEE Signal Processing Letters*, vol. 24, no. 12, pp. 1763–1767, 2017.
- [25] Q. Zhang, Q. Yuan, J. Li, Z. Yang, and X. Ma, "Learning a Dilated Residual Network for SAR Image Despeckling," *Remote Sensing*, vol. 10, no. 2, p. 196, 2018.
- [26] N. Merkle, W. Luo, S. Auer, R. Müller, and R. Urtasun, "Exploiting Deep Matching and SAR Data for the Geo-Localization Accuracy Improvement of Optical Satellite Images," *Remote Sensing*, vol. 9, no. 6, p. 586, Oct. 2017.
- [27] Y. Zhou, H. Wang, F. Xu and Y. Jin, "Polarimetric SAR Image Classification Using Deep Convolutional Neural Networks," in *IEEE Geoscience and Remote Sensing Letters*, vol. 13, no. 12, pp. 1935–1939, Dec. 2016.
- [28] J. Geng, X. Ma, J. Fan and H. Wang, "Semisupervised Classification of Polarimetric SAR Image via Superpixel Restrained Deep Neural Network," in *IEEE Geoscience and Remote Sensing Letters*, vol. 15, no. 1, pp. 122–126, Jan. 2018.
- [29] A. Elmzoughi, R. Abdelfattah and Z. Belhadj, "SAR image classification using the InSAR coherence for soil degradation cartography in the south of Tunisia," *2009 16th IEEE International Conference on Image Processing (ICIP)*, Cairo, 2009, pp. 1677–1680.
- [30] J. Zhao, W. Guo, S. Cui, Z. Zhang and W. Yu, "Convolutional Neural Network for SAR image classification at patch level," *2016 IEEE International Geoscience and Remote Sensing Symposium (IGARSS)*, Beijing, 2016, pp. 945–948.
- [31] C. Danilla, C. Persello, V. Tolpekin and J. R. Bergado, "Classification of multitemporal SAR images using convolutional neural networks and Markov random fields," *2017 IEEE International Geoscience and Remote Sensing Symposium (IGARSS)*, Fort Worth, TX, 2017, pp. 2231–2234.
- [32] Z. Zhang, H. Wang, F. Xu and Y. Jin, "Complex-Valued Convolutional Neural Network and Its Application in Polarimetric SAR Image Classification," in *IEEE Transactions on Geoscience and Remote Sensing*, vol. 55, no. 12, pp. 7177–7188, Dec. 2017.
- [33] T. Crosby, B. Iglewicz, and D. C. Hoaglin, "How to Detect and Handle Outliers," *Technometrics*, vol. 36, no. 3, p. 315, 1994.
- [34] X. Glorot and Y. Bengio, "Understanding the difficulty of training deep feedforward neural networks," in *Proc. Thirteenth Int. Conf. on Artificial Intelligence and Statistics*, May 2010, pp. 249–256.
- [35] N. Otsu, "A Threshold Selection Method from Gray-Level Histograms," in *IEEE Transactions on Systems, Man, and Cybernetics*, vol. 9, no. 1, pp. 62–66, Jan. 1979.
- [36] Y. Boykov, O. Veksler and R. Zabih, "Fast approximate energy minimization via graph cuts," in *IEEE Transactions on Pattern Analysis and Machine Intelligence*, vol. 23, no. 11, pp. 1222–1239, Nov. 2001.
- [37] C. A. Deledalle, L. Denis and F. Tupin, "NL-InSAR: Nonlocal Interferogram Estimation," in *IEEE Transactions on Geoscience and Remote Sensing*, vol. 49, no. 4, pp. 1441–1452, April 2011.
- [38] C. A. Deledalle, L. Denis, F. Tupin, A. Reigber and M. Jäger, "NL-SAR: A Unified Nonlocal Framework for Resolution-Preserving (Pol)(In)SAR Denoising," in *IEEE Transactions on Geoscience and Remote Sensing*, vol. 53, no. 4, pp. 2021–2038, April 2015.